Available online at www.sciencedirect.com
ScienceDirect
Ceramics International 37 (2011) 3049–3054
CERAMICS INTERNATIONAL
www.elsevier.com/locate/ceramint

Microstructure, electrical properties, and aging behavior of $ZnO–Pr_6O_{11}–CoO–Cr_2O_3–Y_2O_3–Er_2O_3$ varistor ceramics

Choon-W. Nahm *

Semiconductor Ceramics Laboratory, Department of Electrical Engineering, Dongeui University, Busan 614-714, Republic of Korea

Received 15 March 2011; received in revised form 29 April 2011; accepted 5 May 2011
Available online 12 May 2011

Abstract

The microstructure, electrical properties, and aging behavior of the $ZnO–Pr_6O_{11}–CoO–Cr_2O_3–Y_2O_3–Er_2O_3$ varistor ceramics were investigated for different contents of Er_2O_3. The microstructure consisted of ZnO grain and an intergranular layer (Pr, Y, and Er-rich phases) as a secondary phase. The increase of Er_2O_3 content decreased the average grain size and increased the sintered density. As the Er_2O_3 content increased, the breakdown field increased from 4206 V/cm to 5857 V/cm and the nonlinear coefficient increased from 32.6 to 48.6. The varistor ceramics added with 1.0 mol% Er_2O_3 exhibited excellent stability by exhibiting −0.2% in the variation rate of the breakdown field and −2.7% in the variation rate of the nonlinear coefficient for aging stress of 0.95 $E_{1\ mA}$/150 °C/24 h.

Keywords: B. Grain boundaries; C. Electrical properties; E. Varistors; Ceramics; Microstructure; Aging behavior

1. Introduction

ZnO-based varistor ceramics possess nonlinear properties, which exhibit abruptly increasing current at a critical value in accordance with increasing voltage. They are manufactured by sintering ZnO added with main subordinate oxides, such as Bi_2O_3 and Pr_6O_{11}, and second subordinate oxide such as CoO, Cr_2O_3, MnO_2, etc. They are monolithic devices consisting of many grains of ZnO, mixed with other materials and compressed into a single form. Highly nonlinear properties enable ZnO ceramics to be used widely in overvoltage protection systems from electronic circuits to electric power systems [1,2]. Most of commercial ZnO varistor ceramics are added with Bi_2O_3 and they exhibit excellent nonlinear properties. However, they have a few flaws due to the high volatility and reactivity of Bi_2O_3 during liquid sintering [3]. The former changes varistor characteristics with the variation of inter-composition ratio of additives, the latter destroys the multi-layer structure of chip varistors, and it generates an insulating spinel phase. This phase acts as a growth moderator for ZnO grain, but plays no role in the nonlinear characteristics [4]. Furthermore, it may also deteriorate the surge-absorption capabilities because the secondary phase such as spinel phases decrease the effective grain boundary area. For this reason, $ZnO–Pr_6O_{11}$-based ceramics have been studying [5–10].

Recently, $ZnO–Pr_6O_{11}$-based varistor ceramics are being studied to further enhance varistor properties and stability against various stresses, such as DC-accelerated aging stress and impulse stress [11–19]. Nahm et al. [11,13–19] reported that $ZnO–Pr_6O_{11}–CoO–Cr_2O_3$-based varistor ceramics doped with rare earth oxides (Er, Y, Dy, La, and Tb) have highly nonlinear properties and high stability against various stresses. These varistor ceramics are limited to five components. To develop varistor ceramics for high performance and wide band applications, it is important to comprehend the effects of the additives on nonlinear properties and stability against the stress. In the present study, the effect of Er_2O_3 addition on the microstructure, electrical properties, and aging behavior of the $ZnO–Pr_6O_{11}–CoO–Cr_2O_3–Y_2O_3–Er_2O_3$ varistor ceramics consisting of six components was investigated and some new results were obtained.

2. Experimental procedure

2.1. Sample preparation

Reagent-grade raw materials were used in proportions of $(97.5 - x)$ mol% ZnO, 0.5 mol% Pr_6O_{11}, 1.0 mol% CoO,

* Tel.: +82 51 890 1669; fax: +82 51 890 1664.
E-mail address: cwnahm@deu.ac.kr.

0272-8842/$36.00
doi:10.1016/j.ceramint.2011.05.032

0.5 mol% Cr_2O_3, 0.5 mol% Y_2O_3, and x mol% Er_2O_3 (x = 0.25, 0.5, 1.0). Raw materials were mixed by ball milling with zirconia balls and acetone in a polypropylene bottle for 24 h. The mixture was dried at 120 °C for 12 h and calcined in air at 750 °C for 2 h. The calcined mixture was pulverized using an agate mortar/pestle and after 2 wt% polyvinyl alcohol (PVA) binder addition, granulated by sieving through a 100-mesh screen to produce the starting powder. The powder was uniaxially pressed into discs of 10 mm in diameter and 2 mm in thickness at a pressure of 80 MPa. The discs were sintered for 1 h at 1340 °C and furnace-cooled to room temperature. The heating and cooling rates were 4 °C/min. The sintered samples were lapped and polished to 1.0 mm thickness. The final samples were about 8 mm in diameter and 1.0 mm in thickness. Silver paste was coated on both faces of the samples, and the electrodes were formed by heating it at 600 °C for 10 min. The electrodes were 5 mm in diameter.

2.2. Microstructure examination

For microstructure characterization, both surfaces of the samples were lapped and ground with SiC paper and polished with 0.3 μm-Al powder to a mirror-like surface. The polished samples were thermally etched at 1050 °C for 30 min. The surface microstructure was examined by a scanning electron microscope (SEM, Hitachi S2400; Chiyoda-Ku, Tokyo, Japan). The average grain size (d) was determined by the lineal intercept method, given by $d = 1.56\,L/MN$, where L is the random line length on the micrograph, M is the magnification of the micrograph, and N is the number of grain boundaries intercepted by the lines [20]. The compositional analysis of the selected areas was determined by an energy dispersion X-ray spectroscope (EDS) attached to the SEM unit. The crystalline phases were identified by an X-ray diffractometer (XRD, Rigaku D/max 2100, Shibuya-Ku, Tokyo, Japan) using a CuK_α radiation. The sintered density (ρ) was measured using a density determination kit (238490) attached to a balance (Mettler Toledo AG 245, Mettler Toledo International Inc., Greifensee, Switzerland).

2.3. Electrical measurement

The electric field–current density (E–J) characteristics were measured using a high voltage source-measure unit (Keithley 237; Keithley Instruments Inc., Cleveland, OH, USA). The breakdown field (E_{1mA}) was measured at 1.0 mA/cm^2, and the leakage current density (J_L) was measured at 0.8 E_{1mA}. In addition, the nonlinear coefficient (α) is defined by the empirical law, $J = C\,E^\alpha$, where J is the current density, E is the applied electric field, and C is a constant. α was determined in the current density range of 1.0–10 mA/cm^2, where $\alpha = 1/(\log E_2 - \log E_1)$, and E_1 and E_2 are the electric fields corresponding to 1.0 mA/cm^2 and 10 mA/cm^2, respectively.

2.4. DC-accelerated aging stress test

The DC-accelerated aging stress test was performed under four continuous conditions;

(i) The 1st stress: 0.85 $E_{1\ mA}$/115 °C/24 h, (ii) the 2nd stress: 0.90 $E_{1\ mA}$/120 °C/24 h, (iii) the 3rd stress: 0.95 $E_{1\ mA}$/125 °C/24 h, and (iv) the 4th stress: 0.95 $E_{1\ mA}$/150 °C/24 h.

The leakage current was monitored at intervals of 1 min during stressing using a high voltage source-measure unit (Keithley 237). The degradation rate coefficient (K_T) was calculated from the expression $I_L = I_{Lo} + K_T t^{1/2}$ [21], where I_L is the leakage current at stress time (t), and I_{Lo} is I_L at $t = 0$. After the respective stresses, the E–J characteristics were measured at room temperature.

3. Results and discussion

Fig. 1 shows SEM micrographs of the samples for different contents of Er_2O_3. The microstructure consisted of ZnO grain as a primary phase and an intergranular layer as a secondary phase. The XRD patterns indicated in Fig. 2 revealed the presence of Pr_6O_{11}, Y_2O_3, and Er_2O_3-rich intergranular layer as minor secondary phases, in addition to a major phase of hexagonal ZnO. The EDS spectra in Fig. 3 show that the Pr_6O_{11}, Y_2O_3, and Er_2O_3 are segregated at grain boundaries and nodal points due to an ionic radius difference for Zn, and coexist in the grain boundaries and the nodal points as if they were a single phase. The sintered density (ρ) increased from 5.46 g/cm^3 to 5.56 g/cm^3 (5.78 g/cm^3 in pure ZnO) with the increase of Er_2O_3 content. The average grain size (d) decreased from 6.5 μm to 5.6 μm. Therefore, the densification of the samples is enhanced by the addition of Er_2O_3. The detailed microstructural parameters are summarized in Table 1.

Fig. 4 shows the E–J characteristics of the samples for different contents of Er_2O_3. The curves show that the conduction characteristics are divided into a linear region with very high impedance before breakdown field and a nonlinear region with very low impedance after breakdown field. A sharper knee on the curves between the two regions indicates better nonlinear properties. However, the knee states of these curves are not distinguished by the content of Er_2O_3. The Er_2O_3 content shifted the electric field curves to lower field strengths. Therefore, Er_2O_3 addition had a strong effect on the E–J characteristics.

The breakdown field ($E_{1\ mA}$) greatly increased from 4206 V/cm to 5857 V/cm with the increase of Er_2O_3. The samples relatively provide a high breakdown field per unit thickness. This is very effective for high voltage varistors with a compact size. The increase of $E_{1\ mA}$ with the increase of Er_2O_3 content can be explained by the increase in the number of grain boundaries due to the decrease of average ZnO grain size as follows: $E_{1\ mA} = v_{gb}/d$, where v_{gb} is the breakdown voltage per grain boundary, and d is the average grain size. The v_{gb} values of the samples added with Er_2O_3 were within the normal range of values of 2–4 V/gb. As a result, the $E_{1\ mA}$ is significantly affected by the average grain size with the increased content of Er_2O_3.

The nonlinear coefficient (α) increased from 32.6 to 48.6 with the increase of Er_2O_3 content. It can be seen that the Er_2O_3 addition has a significant effect on the nonlinear properties in

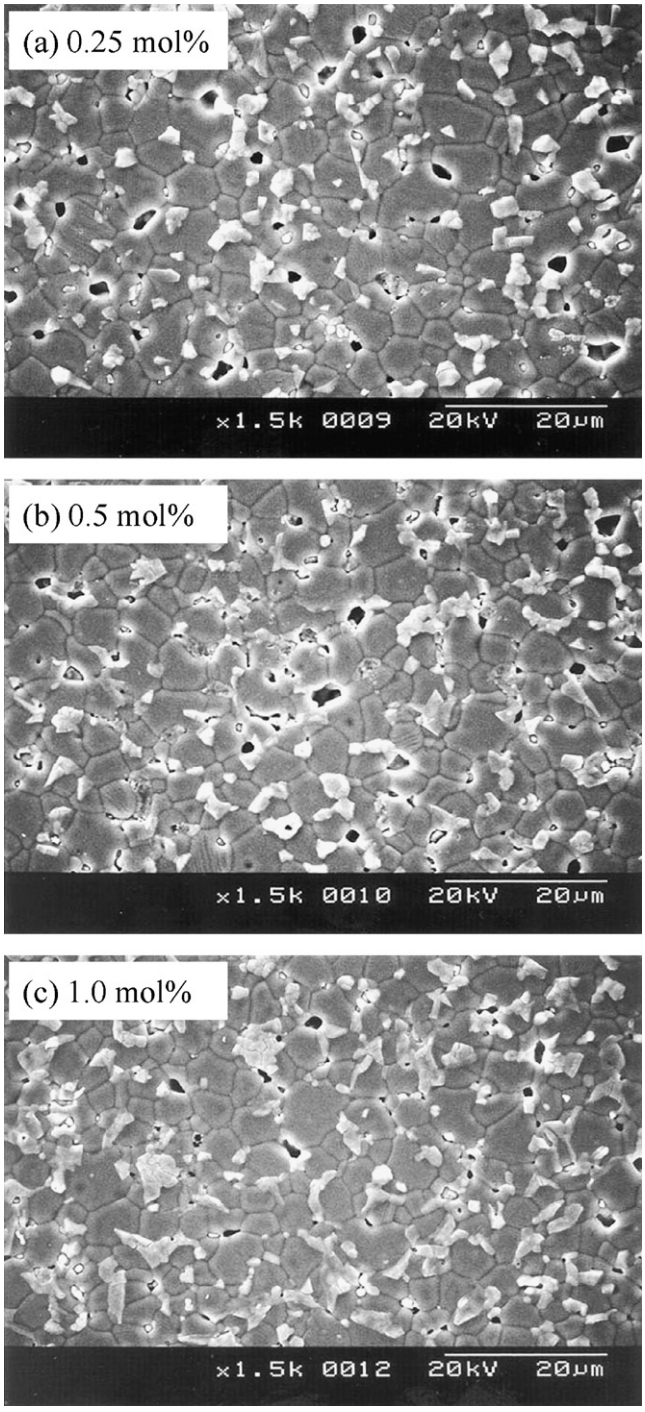

Fig. 1. SEM micrographs of the samples for different contents of Er_2O_3.

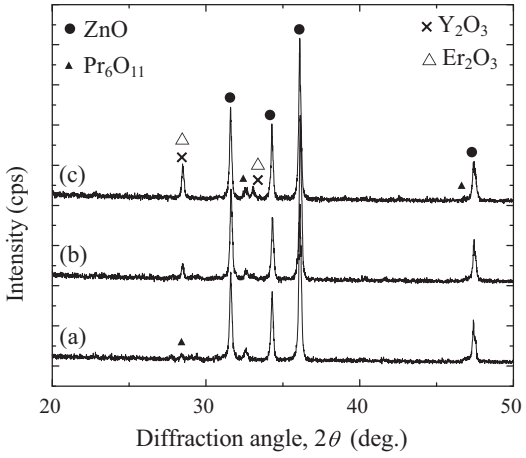

Fig. 2. XRD patterns of the samples for different contents of Er_2O_3: (a) 0.25 mol%, (b) 0.5 mol%, and (c) 1.0 mol%.

the light of the α variation. The behavior of α with Er_2O_3 content can be related to the variation of the Schottky barrier height according to the variation of the electronic states at the grain boundaries. The Er_2O_3 addition will vary the density of the interface states with the transport of the defect ions toward the grain boundary and will be more active grain boundaries. Therefore, the increase of α in accordance with Er_2O_3 content is attributed to the increase of potential barrier height at the grain boundaries. The J_L increased remarkably from 2.1 $\mu A/cm^2$ to 0.8 $\mu A/cm^2$ with the increase of Er_2O_3 content. The variation of J_L shows an inverse relationship to the variation of α in accordance with the content of Er_2O_3. As a result, it was found that the addition of Er_2O_3 remarkably improves the *E–J* characteristics; namely, it increases the nonlinear coefficient and decreases the leakage current. It is clear that the values of α and J_L were strongly affected by the content of Er_2O_3. The detailed electrical parameters are summarized in Table 1.

The electronic and communication equipment and the electrical power system demand high stability from the varistors in order to enhance their reliability. In practice, the ZnO varistors are always subjected to external stress, such as DC, AC, surge, etc. The aging progresses gradually. Therefore, the electrical stability together with nonlinearity is an important characteristic of ZnO varistors [11].

Fig. 5 shows the leakage current behavior of the samples during various DC-accelerated aging stresses in accordance with the content of Er_2O_3. The samples added with 0.25 mol% Er_2O_3 exhibited high stability at the third stress (0.95 $E_{1\ mA}$/125 °C/24 h). However, they exhibited instability at the fourth stress (0.95 $E_{1\ mA}$/150 °C/24 h), which gives rise to a thermal runaway. It is assumed that the thermal runaway of the samples

Table 1
Microstructure and *E–J* characteristic parameters for the samples for different contents of Er_2O_3.

Er_2O_3 content (mol%)	d (μm)	ρ (g/cm^3)	$E_{1\ mA}$ (V/cm)	v_{gb} (V/gb)	α	J_L (μA/cm^2)
0.25	6.5	5.46	4206	2.7	32.6	2.1
0.5	5.9	5.40	5172	3.0	43.2	1.2
1.0	5.6	5.56	5857	3.3	48.6	0.8

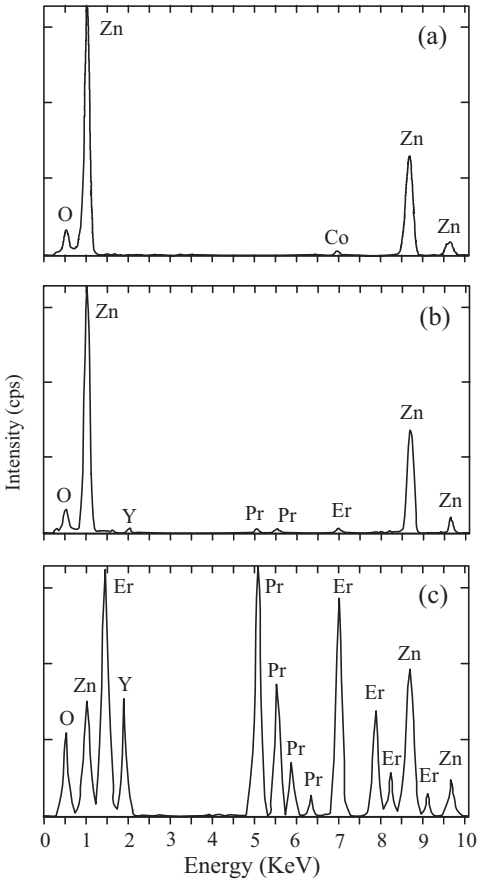

Fig. 3. EDS spectra of the samples: (a) ZnO grain, (b) grain boundary, and (c) intergranular layer.

added with 0.25 mol% Er_2O_3 is attributed to a low sintered density and high leakage current density. A low sintered density decreases the number of conduction paths, and eventually leads to the concentration of current. Furthermore, a high leakage current leads to high joule heat loss. On the other hand, the samples added with 0.5 mol% and 1.0 mol% Er_2O_3 exhibited a much higher stability than the samples added with 0.25 mol% Er_2O_3. This is attributed to a comparatively high sintered density and low leakage current. The stability of the varistors can be estimated by the degradation rate coefficient (K_T), which indicates the degree of aging. This exhibits the slope of the

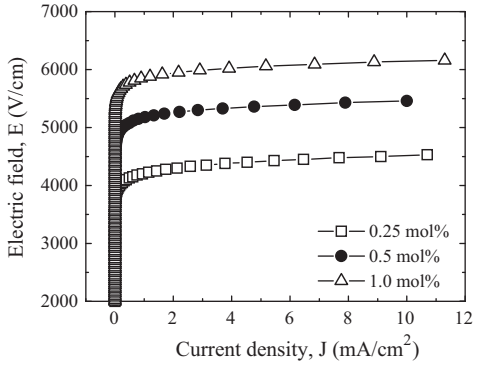

Fig. 4. *E–J* characteristics of the samples for different contents of Er_2O_3.

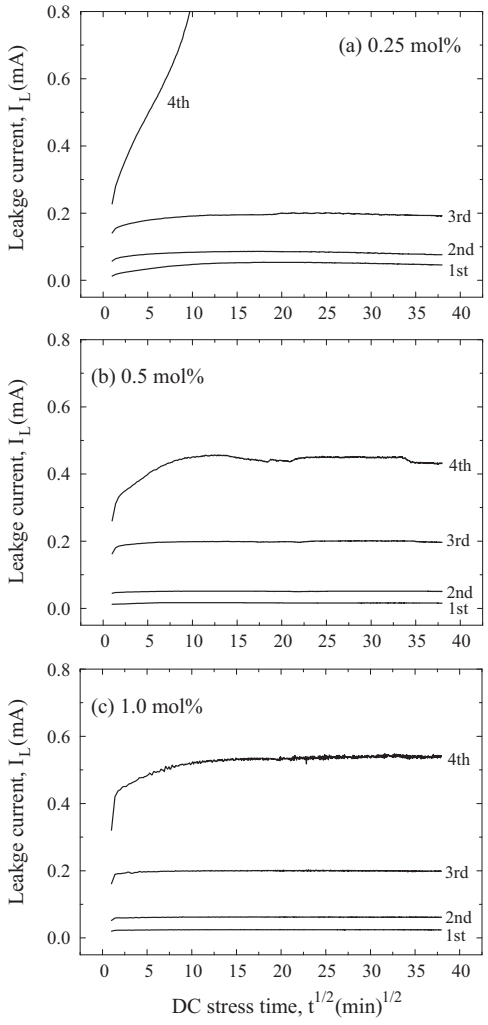

Fig. 5. Leakage current behavior during applying the stress of the samples for different contents of Er_2O_3.

leakage current for the stress time. In general, lower K_T values indicate greater stability, whereas it is not absolute estimation degree for stability. The K_T of each sample in accordance with the content of Er_2O_3 is exhibited in Fig. 6. The K_T of the samples added with 0.5 mol% and 1.0 mol% Er_2O_3 is

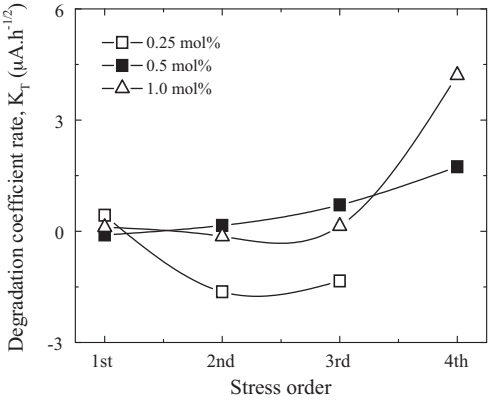

Fig. 6. Degradation coefficient rate of the samples for different contents of Er_2O_3.

0.71 μA $h^{-1/2}$ and 0.14 μA $h^{-1/2}$ at the third stress (0.95 $E_{1\ mA}$/125 °C/24 h), respectively. The samples added with 1.0 mol% exhibited lower K_T value than that of the samples added with 0.5 mol% up to the third stress. However, after the fourth stress the samples added with 0.5 mol% exhibited the lowest K_T value. It is presumed that the samples added with 0.5 mol% exhibited a slightly greater stability than the samples added with 1.0 mol%. The experimental facts indicate that the resistance against the DC-accelerated aging stress is greatly affected by the content of Er_2O_3.

Fig. 7 compares the variation of *E–J* characteristics after applying the DC-accelerated aging stress with the initial *E–J* characteristics in accordance with the content of Er_2O_3. Among the *E–J* curves after the stress is applied, those of the linear region moved toward a higher current density. The degree of variation of *E–J* curves in the linear region was the largest for the samples added with 0.25 mol% Er_2O_3 and was smaller for the samples added with 0.5 and 1.0 mol% Er_2O_3. Therefore, the variation of *E–J* characteristics after applying the DC-accelerated aging stress coincided with the variation of the K_T value. Table 2 summarizes the *E–J* characteristic parameters, such as the variation rates of the breakdown field ($\%\Delta E_{1\ mA}$), nonlinear coefficient ($\%\Delta\alpha$), and leakage current ($\%\Delta J_L$) after applying the DC-accelerated aging stress. The samples added with 0.5 mol% and 1.0 mol% Er_2O_3 exhibited low characteristic variation of −0.4% and −0.2% in $\%\Delta E_{1\ mA}$, respectively, and −5.3% and −2.7% in $\%\Delta\alpha$, respectively after the fourth stress (0.95 $E_{1\ mA}$/150 °C/24 h). Based on $\%\Delta E_{1\ mA}$ and $\%\Delta\alpha$, it is clear that the samples added with 1.0 mol% is more stable than the samples added with 0.5 mol%. On the other hand, the leakage current greatly increased after applying the fourth stress. The $\%\Delta J_L$ for both samples is very high variation, compared with $\%\Delta E_{1\ mA}$ and $\%\Delta\alpha$ after applying the fourth stress. These samples showed a much higher stability than those of the samples without Er_2O_3 reported previously [9]. On the whole, it is carefully confirmed that the optimal Er_2O_3 content for sintering temperature of 1340 °C in the ZnO–Pr_6O_{11}–CoO–Cr_2O_3–Y_2O_3–Er_2O_3 varistor ceramics may be 1.0 mol%.

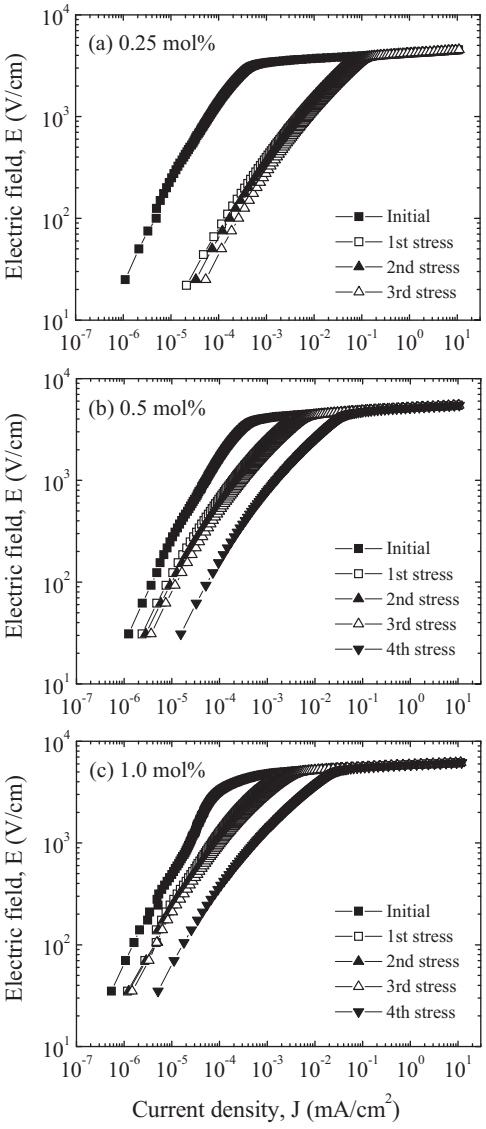

Fig. 7. *E–J* characteristic behavior during applying the stress of the samples for different contents of Er_2O_3.

Table 2
E–J characteristic parameters after DC-accelerated aging stress for the samples for different contents of Er_2O_3.

Er_2O_3 content (mol%)	Stress state	$E_{1\ mA}$ (V/cm)	$\%\Delta E_{1\ mA}$	α	$\%\Delta\alpha$	J_L (μA/cm²)	$\%\Delta J_L$
0.25	Initial	4206	–	32.6	–	2.1	–
	1st	4197	−0.2	31.2	−4.3	54.3	2486
	2nd	4194	−0.3	31.4	−3.7	59.1	2714
	3rd	4186	−0.5	30.8	−5.5	87.4	4062
	4th	Thermal runaway					
0.5	Initial	5172	–	43.2	–	1.2	–
	1st	5169	−0.1	42.8	−0.9	4.2	250
	2nd	5168	−0.1	42.7	−1.1	5.0	317
	3rd	5160	−0.2	42.0	−2.8	6.6	450
	4th	5149	−0.4	40.9	−5.3	33.5	2692
1.0	Initial	5857	–	48.6	–	0.8	–
	1st	5856	−0.0	48.2	−0.8	2.1	162
	2nd	5854	−0.1	48.0	−1.2	2.6	225
	3rd	5851	−0.1	47.7	−1.8	3.6	350
	4th	5843	−0.2	47.3	−2.7	20.0	2400

4. Conclusions

The microstructure, electrical properties, and aging behavior of the ZnO–Pr_6O_{11}–CoO–Cr_2O_3–Y_2O_3–Er_2O_3 varistor ceramics were investigated for different contents of Er_2O_3. The microstructure consisted of ZnO grain and an intergranular phase (Pr, Y, and Er-rich phase) as a secondary phase. As the Er_2O_3 content increased, the breakdown field increased from 4206 V/cm to 5857 V/cm, and the nonlinear coefficient increased from 32.6 to 48.6. The varistor ceramics added with 1.0 mol% Er_2O_3 exhibited excellent stability by exhibiting −0.2% in the variation rate of the breakdown field and −2.7% in the variation rate of the nonlinear coefficient for aging stress of 0.95 $E_{1\ mA}$/150 °C/24 h. These varistor ceramics could be applied to the compact type with high voltage gradient, because they provide not only a nonlinear coefficient greater than 45, but also a high breakdown field greater than 5000 V/cm.

References

[1] L.M. Levinson, H.R. Philipp, Zinc oxide varistor – a review, Am. Ceram. Soc. Bull. 65 (1986) 639–646.

[2] T.K. Gupta, Application of zinc oxide varistor, J. Am. Ceram. Soc. 73 (1990) 1817–1840.

[3] Y.S. Lee, T.Y. Tseng, Phase identification and electrical properties in ZnO–glass varistors, J. Am. Ceram. Soc. 75 (1992) 1636–1640.

[4] J. Wong, Microstructure and phase transformation in a highly non-Ohmic metal oxide varistor ceramic, J. Appl. Phys. 46 (1975) 1653–1659.

[5] K. Mukae, K. Tsuda, I. Nagasawa, Non-ohmic properties of ZnO–rare earth metal oxide–Co_3O_4 ceramics, Jpn. J. Appl. Phys. 16 (1977) 1361–1368.

[6] K. Mukae, Zinc oxide varistors with praseodymium oxide, Am. Ceram. Soc. Bull. 66 (1987) 1329–1331.

[7] H.K. Varma, K.P. Kumar, K.G.K. Warrier, A.D. Damodaran, Effect of K_2O on the sintered microstructure of praseodymium-doped ZnO varistors, J. Mater. Sci. Lett. 8 (1989) 974–976.

[8] A.B. Alles, V.L. Burdick, The effect of liquid-phase sintering on the properties of Pr_6O_{11}-based ZnO varistors, J. Appl. Phys. 70 (1991) 6883–6890.

[9] A.B. Alles, R. Puskas, G. Callahan, V.L. Burdick, Compositional effects on the liquid-phase sintering of praseodymium oxides-based zinc oxides varistors, J. Am. Ceram. Soc. 76 (1993) 2098–2102.

[10] Y.-S. Lee, K.-S. Liao, T.-Y. Tseng, Microstructure and crystal phases of praseodymium in zinc oxide varistor ceramics, J. Am. Ceram. Soc. 79 (1996) 2379–2384.

[11] C.-W. Nahm, The nonlinear properties and stability of ZnO–Pr_6O_{11}–CoO–Cr_2O_3–Er_2O_3 ceramic varistors, Mater. Lett. 47 (2001) 182–187.

[12] H.H. Hng, K.M. Knowles, Microstructure and current–voltage characteristics of praseodymium-doped zinc oxide varistors containing MnO_2, Sb_2O_3 and Co_3O_4, J. Mater. Sci. 37 (2002) 143–1154.

[13] C.-W. Nahm, B. Shin, M.-H. Min, Microstructure and electrical properties of Y_2O_3-doped ZnO–Pr_6O_{11}-based varistor ceramics, Mater. Chem. Phys. 82 (2003) 157–164.

[14] C.-W. Nahm, B.-C. Shin, Effect of sintering time on electrical properties and stability against DC accelerated aging of Y_2O_3-doped ZnO–Pr_6O_{11}-based varistor ceramics, Ceram. Int. 30 (2004) 9–15.

[15] C.-W. Nahm, Electrical properties and stability against DC accelerated aging stress of ZPCCE-based varistor ceramics, J. Mater. Sci. Mater. Electron. 15 (2004) 29–36.

[16] C.-W. Nahm, B.-C. Shin, Effect of sintering time on electrical characteristics and DC accelerated aging behaviors of Zn–Pr–Co–Cr–Dy oxide-based varistors, J. Mater. Sci. Mater. Electron. 16 (2005) 725–732.

[17] C.-W. Nahm, Effect of sintering temperature on nonlinear electrical properties and stability against DC accelerated aging stress of (CoO, Cr_2O_3, La_2O_3)-doped ZnO–Pr_6O_{11}-based varistors, Mater. Lett. 60 (2006) 3311–3314.

[18] C.-W. Nahm, Electrical properties and aging characteristics of terbium-doped ZPCC-based varistors, Mater. Sci. Eng. B 137 (2007) 112–118.

[19] C.-W. Nahm, Electrical behavior against current impulse in ZnO–Pr_6O_{11}-based varistor ceramics with terbium addition, Ceram. Int. 36 (2010) 1495–1501.

[20] J.C. Wurst, J.A. Nelson, Lineal intercept technique for measuring grain size in two-phase polycrystalline ceramics, J. Am. Ceram. Soc. 55 (1972) 109–111.

[21] J. Fan, R. Freer, Deep level transient spectroscopy of zinc oxide varistors doped with aluminum oxide and/or silver oxide, J. Am. Ceram. Soc. 77 (1994) 2663–2668.